$L_4Fe_2As_2Te_{1-x}O_{4-y}F_y$ (L = Pr, Sm, Gd): A layered oxypnictide superconductor with T_c up to 45 K

S. Katrych,[1,*] A. Pisoni,[1] S. Bosma,[2] S. Weyeneth,[2] N. D. Zhigadlo,[3] R. Gaal,[1] J. Karpinski,[1,3] and L. Forró[1]

[1]*Institute of Condensed Matter Physics, EPFL, CH-1015 Lausanne, Switzerland*

[2]*Physik-Institut der Universität Zürich, Winterthurerstrasse 190, CH-8057 Zürich, Switzerland*

[3]*Laboratory for Solid State Physics, ETH Zurich, CH-8093 Zurich, Switzerland*

(Received 21 November 2013; revised manuscript received 18 December 2013; published 31 January 2014)

The synthesis and structural and physical properties of iron lanthanide oxypnictide superconductors, $L_4Fe_2As_2Te_{1-x}O_4$ (L = Pr, Sm, Gd), with transition temperature at ~25 K are reported. Single crystals have been grown at high pressure using the cubic anvil technique. The crystal structure consists of layers of L_2O_2 tetrahedra separated by alternating layers of chains of Te and of Fe_2As_2 tetrahedra: -L_2O_2-Te-L_2O_2-Fe_2As_2-L_2O_2-Te-L_2O_2- (space group: $I4/mmm$, $a \sim 4.0$, $c \sim 29.6$ Å). Substitution of oxygen by fluorine increases the critical temperature, e.g., in $Gd_4Fe_2As_2Te_{1-x}O_{4-y}F_y$ up to 45 K. Magnetic torque measurements reveal an anisotropy of the penetration depths of ~31.

DOI: 10.1103/PhysRevB.89.024518 PACS number(s): 81.10.−h, 74.62.Bf, 74.70.Xa, 74.25.−q

I. INTRODUCTION

The discovery of high-temperature superconductivity in $LaFeAsO_{1-x}F_x$ [1] has spiraled up an investigation of a variety of compounds consisting of M_2As_2 (M is a transition metal) layers alternating with L_2O_2 (L is a lanthanide metal) layers or metal layers (e.g., Ba, Li, or other). In view of the fact that all of these compounds were reported already before discovery of superconductivity in La1111 [2,3], and their synthesis procedure as well as structure details were well investigated, great progress in finding several new iron-based superconductors was achieved by doping of known layered pnictides and oxypnictides in less than one year. Superconductivity was also found in FeSe or "11" (T_c = 8 K) [4,5], $Ba_{1-x}K_xFe_2As_2$ or "122" (T_c = 38 K) [6,7], LiFeAs or "111" (T_c = 18 K) [8,9], and $La_3Ni_4P_4O_2$ or "3442" (T_c = 2.2 K) [10,11].

In this paper, we present the systematic study of superconducting compounds $L_4Fe_2As_2Te_{1-x}O_4$ (L = Pr, Sm, Gd) with a hitherto unknown structure. Our recent work [12], where crystal growth, structure, and physical properties of an oxypnictide superconductor $Pr_4Fe_2As_2Te_{1-x}O_4$ with a critical temperature (T_c) close to 25 K were reported, triggered this study with the intention of increasing T_c of this compound.

The structure of $Pr_4Fe_2As_2Te_{1-x}O_4$ (also called 42214) reveals the same structural blocks as the PrFeAsO (1111) oxypnictide superconductor [3]: fluorite-type Pr_2O_2 layers alternating with anti-fluorite-type Fe_2As_2 layers with a difference in the presence of intercalated Te atoms [Fig. 1(a)–1(c)]. Both structures are tetragonal with the space group $I4/mmm$ for the former and $P4/nmm$ for the latter.

For the 1111 phase, two parameters are known to increase T_c by modifying the structure or composition. One of them is pnictogen height h_P (half of the thickness of the Fe_2As_2 or S_2, [Fig. 1(a)–1(c)], which, as an indicator for highest possible T_c, should be close to 1.38 Å [13,14]. The LFeAsO for L = Sm and Gd have h_P values close to the "optimal" one.

The other factor is doping. The pure stoichiometric, undoped 1111 phase does not reveal superconductivity [1]. The most effective doping that results in T_c above 50 K is at the oxygen sites, either by fluorine, hydrogen, or by oxygen vacancies [1,15,16]. Substitution of Sm by Th also leads to T_c above 50 K [17,18].

According to our recent investigations [12,19], the lattice constants a and b, Fe_2As_2 layer thickness S_2, and Fe_2As_2-L_2O_2 interlayer distance S_3 are almost equal for both PrFeAsO and for $Pr_4Fe_2As_2Te_{1-x}O_4$ (Fig. 1(a)–1(c)). In analogy to 1111, one can expect that "optimal" h_P and proper doping should lead to high T_c in 42214 compounds. $L_4Fe_2As_2Te_{1-x}O_4$ (L = Sm and Gd) doped with fluorine, as one of the options, was assumed to be the ideal candidate for increasing T_c in 42214 because h_P of LFeAsO (L = Sm, Gd) corresponds to the maximal T_c. To prove this suggestion, a detailed structural study of undoped $L_4Fe_2As_2Te_{1-x}O_4$ (L = Pr, Sm, Gd) was performed, and the influence of fluorine substitution for oxygen on T_c in $L_4Fe_2As_2Te_{1-x}O_4$ (L = Sm, Gd) was studied.

Here, we report on the high-pressure crystal growth, structure, and doping of $L_4Fe_2As_2Te_{1-x}O_{4-y}F_y$ (L = Pr, Sm, Gd) single crystals. The critical temperature of Gd42214 single crystals increased after F doping from 25 K up to 45 K.

II. EXPERIMENTAL DETAILS

The crystals of $Pr_4Fe_2As_2Te_{1-x}O_4$, $Sm_4Fe_2As_2Te_{1-x}O_{4-y}F_y$, and $Gd_4Fe_2As_2Te_{1-x}O_{4-y}F_y$ were grown at high pressure from precursors (presintered mixture of 0.9PrAs + 0.1PrTe + FeO, 0.9SmAs + 0.1TeO_2 + 0.5FeO + 0.15FeF_2 + 0.35Fe + 0.1Sm and Fe + 0.9GdAs + 0.1GdTe + 0.8FeO + 0.1FeF_2, respectively) in NaCl/KCl flux. The procedure is described by Katrych *et al.* [12]. The same procedure was used for the growth of $L_4Fe_2As_2Te_{1-x}O_4$ (L = Sm, Gd) crystals from stoichiometric mixture of high-purity (⩾99.95%) L, LAs, FeO, and TeO_2.

The single crystals were studied on a three-circle x-ray diffractometer equipped with a CCD detector (Bruker AXS Inc.). Data reduction and multiscan absorption correction were performed using the APEX2 [20] and SAINT [21] software. The crystal structure was solved by a direct method, and the full

*Corresponding author: sergiy.katrych@epfl.ch

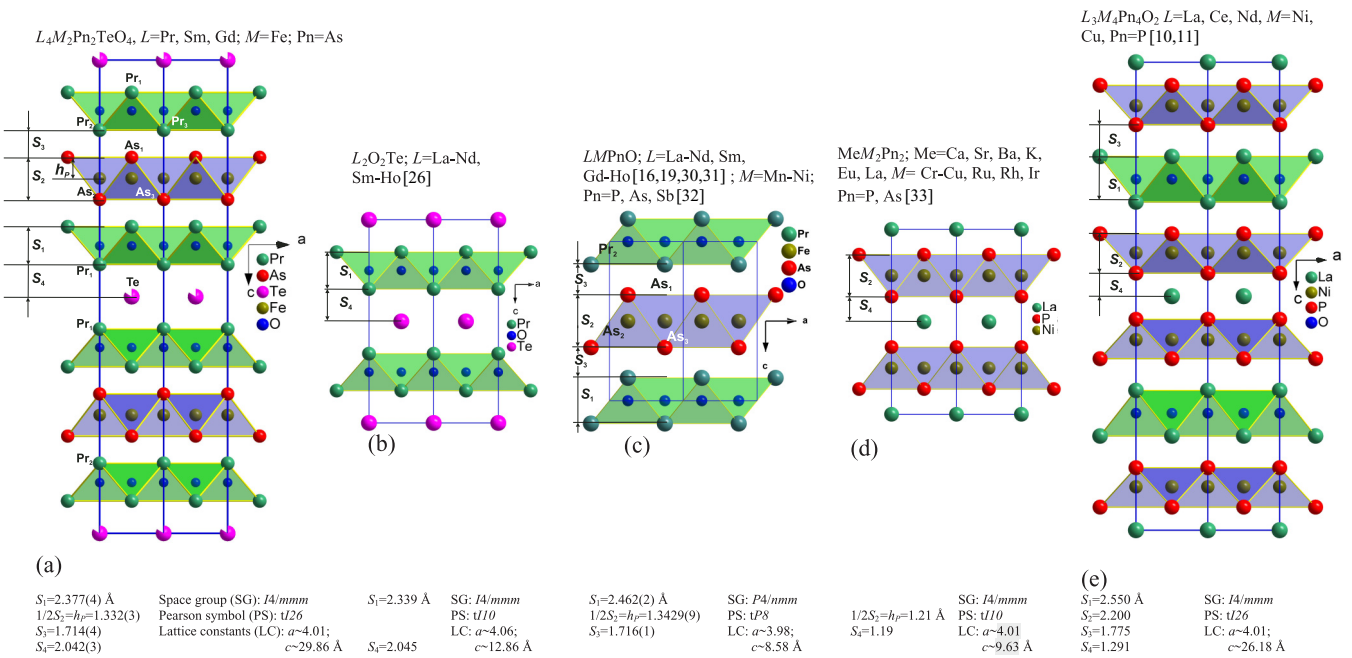

FIG. 1. (Color online) 1 × 2 unit cell projection in the *ac* plane (along *b* direction) from left to right: (a) $L_4M_2Pn_2TeO_4$; (b) L_2O_2Te; (c) LMPnO; (d) LM_2Pn_2; (e) $L_3M_4Pn_4O_2$.

data set was refined on F^2, employing the programs SHELXS-97 [22] and SHELXL-97 [23].

The magnetization as a function of temperature has been measured for individual single crystals of $L_4Fe_2As_2Te_{1-x}O_4$ (L = Pr, Gd) and $L_4Fe_2As_2Te_{1-x}O_{4-y}F_y$ (L = Sm, Gd) doped with fluorine. These experiments have been done with a magnetic property measurement system (MPMS) with enhanced sensitivity (MPMS-XL).

Because individual $Sm_4Fe_2As_2Te_{1-x}O_4$ single crystals were too small, the magnetic susceptibility χ_ρ measurement was performed on a powdered sample using an MPMS (Quantum Design) under zero-field-cooling (ZFC) and field-cooling (FC) conditions.

The electrical resistivity (ρ) of a $Sm_4Fe_2As_2Te_{1-x}O_{4-y}F_y$ single crystal was measured as a function of temperature using a standard four-probe method. Gold wires of 12 μm diameter were glued with silver paint on a 150-μm-long sample in a van der Pauw geometry. The contact resistance was less than 200 Ω. A sensing current of 100 μA was generated using a Keithley 220 programmable current source, and the resulting signal was measured by a Keithley 2182 nanovoltmeter. The sample was cooled in a liquid helium bath cryostat from room temperature at a rate of 0.5 K/min.

The magnetic anisotropy measurements were carried out with a homemade magnetic torque sensor [24]. A tiny $Sm_4Fe_2As_2Te_{1-x}O_{4-y}F_y$ single crystal (~100 × 100 × 10 μm^3) was fixed on a platform hanging on piezoresistive legs. When a static magnetic field was applied to this anisotropic superconductor, a torque proportional to the vector product of magnetization and field appears and bends the piezoresistive legs. The resulting change in resistance can be read out electronically, yielding a signal proportional to the torque [24].

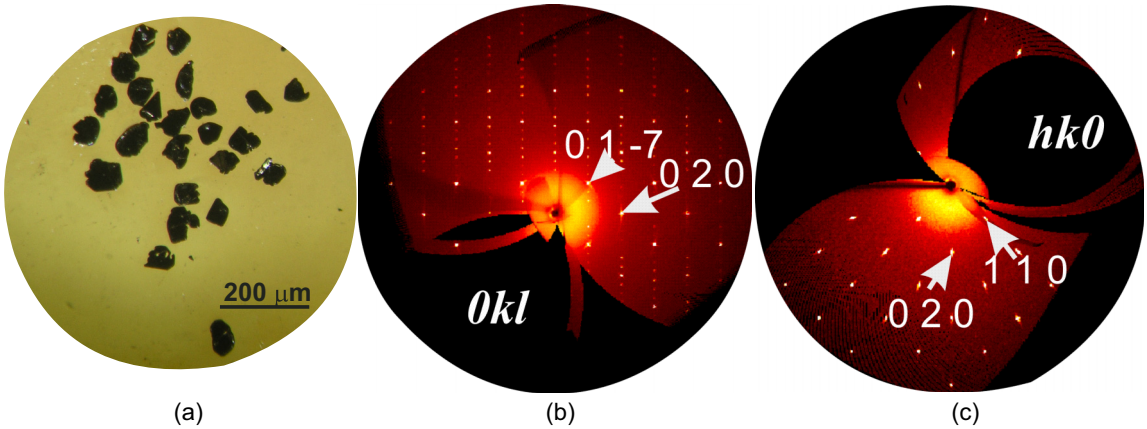

FIG. 2. (Color online) (a) Single crystals of $Pr_4Fe_2As_2Te_{1-x}O_4$. (b) and (c): The reconstructed (*0kl*) and (*hk0*) reciprocal space sections for $Pr_4Fe_2As_2Te_{1-x}O_4$.

TABLE I. Details of the structure refinement for the $L_4Fe_2As_2Te_{1-x}O_4$ (L = Pr, Sm, Gd) crystals. The diffraction study is performed at 295(2) K using Mo K_α radiation with $\lambda = 0.71073$ Å. The lattice is tetragonal, space group is $I4/mmm$, $Z = 2$. A full-matrix least-squares method was employed to optimize F^2.

Empirical formula	$Pr_4Fe_2As_2Te_{0.88(1)}O_4$	$Sm_4Fe_2As_2Te_{0.92(1)}O_4$	$Gd_4Fe_2As_2Te_{0.90(1)}O_4$
T_c, K	25	25	25
Unit cell dimensions, Å	$a = 4.0165(2)$, $c = 29.8572(16)$	$a = 3.9642(3)$, $c = 29.509(2)$	$a = 3.9353(3)$, $c = 29.369(3)$
Volume, Å^3	481.66(4)	463.74(6)	454.82(7)
L_1-L_2, Å	3.7026(6)	3.6278(4)	3.5928(8)
O-O = Fe-Fe, Å	2.84009(14)	2.8031(2)	2.7827(2)
L_2-As_1/L_1-Te, Å	3.3176(7)/3.4986(4)	3.2718(6)/3.4638(3)	3.2438(10)/3.4485(5)
L_2-O/L_1-O, Å	2.346(2)/2.320(3)	2.305(2)/2.2802(19)	2.284(4)/2.261(4)
As_1-As_2, Å	3.8922(12)	3.8953(9)	3.8992(18)
Fe-As, Å	2.4091(7)	2.3995(5)	2.3952(10)
As_1-Fe-As_2, β (°)	107.77(2)	108.521(17)	108.97(3)
As_2-Fe-As_3, α (°)	112.94(5)	111.39(4)	110.47(7)
S_1, Å	2.377(4)	2.302(4)	2.273(4)
$1/2S_2/h_P$, Å	1.332(3)	1.352(3)	1.366(3)
Fig. 1(a)			
S_3, Å	1.714(4)	1.688(4)	1.668(4)
S_4, Å	2.042(3)	2.036(3)	2.035(3)
Calculated density, g/cm^3	6.901	7.484	7.809
Absorption coefficient, mm^{-1}	32.145	37.855	41.860
$F(000)$	863	892	906
Crystal size, mm^3	0.11 × 0.07 × 0.03	0.11 × 0.06 × 0.03	0.11 × 0.08 × 0.03
Theta range for data collection, deg.	2.73 to 45.29	2.76 to 45.22	4.16 to 40.24
Index ranges	$-4 = <h< = 7$, $-7 = <k< = 8$, $-47 = <l< = 59$	$-3 = <h< = 7$, $-6 = <k< = 7$, $-58 = <l< = 57$	$-7 = <h< = 7$, $-7 = <k< = 4$, $-41 = <l< = 52$
Reflections collected/unique	2778/670 $R_{int.} = 0.0363$	3827/640 $R_{int.} = 0.0410$	2986/490 $R_{int.} = 0.0443$
Completeness to 2theta	98.4%	97.3%	97.8%
Data/restraints/parameters	670/0/19	640/0/19	490/0/19
Goodness-of-fit on F^2	1.436	1.224	1.187
Final R indices [I>2sigma(I)]	$R_1 = 0.0374$, w$R_2 = 0.0958$	$R_1 = 0.0298$, w$R_2 = 0.0679$	$R_1 = 0.0410$, w$R_2 = 0.0997$
R indices (all data)	$R_1 = 0.0406$, w$R_2 = 0.0997$	$R_1 = 0.0313$, w$R_2 = 0.0684$	$R_1 = 0.0428$, w$R_2 = 0.1002$

III. RESULTS AND DISCUSSION

A. Structure analysis

The crystals of $Pr_4Fe_2As_2Te_{1-x}O_4$ with plate-like shape reveal nice quality with a mosaic spread of ~1.1° (Fig. 2).

Structure of 42214 (Fig. 1(a)) was determined and refined on the base of 670 independent reflections. Since the displacement parameter of Te was larger than that of other atoms, the occupation parameter for it was set as a free variable. Finally, the Te site reveals about 10% of vacancies [12]. The same Te deficiency was found in $L_4Fe_2As_2Te_{1-x}O_4$ (L = Sm, Gd), which was refined using the $Pr_4Fe_2As_2Te_{1-x}O_4$ structural model. Table I and Table II provide the results of structure determination and refinement.

Despite the entirely different stoichiometric composition or formula type, the determined structure has some resemblance to that of $La_3Cu_4P_4O_2$ [10], or another representative of its structure type, superconducting $La_3Ni_4P_4O_2$ (3442) [11]. The number of atoms in the unit cells as well as the space group are the same (Pearson symbol: tI26, space-group:

TABLE II. Atomic coordinates and equivalent isotropic and anisotropic displacement parameters [Å^2 × 10^3] for the $L_4Fe_2As_2Te_{1-x}O_4$. U_{iso} is defined as one third of the trace of the orthogonalized U_{ij} tensor. The anisotropic displacement factor exponent takes the form: $-2\pi^2$ $[(h^2a^2U_{11} + \cdots + 2hka^*b^*U_{12}]$. For symmetry reasons $U_{23} = U_{13} = U_{12} = 0$.

Atom	Site	x	y	z L = Pr/Sm/Gd	U_{iso}	$U_{11} = U_{22}$	U_{33}
L_1	4e	½	½	0.0684(1)/0.0690(1)/0.0693(1)	9(1)/7(1)/8(1)	8(1)/6(1)/6(1)	11(1)/8(1)/11(1)
L_2	4e	0	0	0.1480(1)/0.1470(1)/0.1467(1)	9(1)/7(1)/8(1)	9(1)/6(1)/7(1)	10(1)/8(1)/10(1)
As	4e	½	½	0.2054(1)/0.2042(1)/0.2035(1)	12(1)/9(1)/12(1)	13(1)/9(1)/13(1)	10(1)/8(1)/9(1)
Te	2a	0	0	0	16(1)/13(1)/17(1)	18(1)/15(1)/20(1)	12(1)/10(1)/12(1)
Fe	4d	½	0	¼	11(1)/9(1)/10(1)	10(1)/8(1)/8(1)	12(1)/10(1)/13(1)
O	8g	½	0	0.1073(2)/0.1072(1)/0.1072(3)	10(1)/8(1)/8(1)	10(2)/6(1)/6(3)	12(2)/12(1)/15(3)

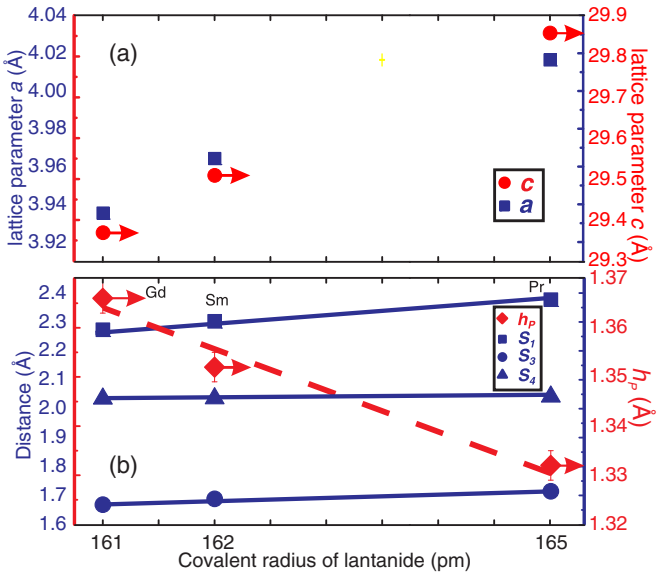

FIG. 3. (Color online) (a) and (b) Lattice parameters and layer thickness with interlayer distances as a function of covalent radius of lanthanide (arrows show that right Y axis should be used).

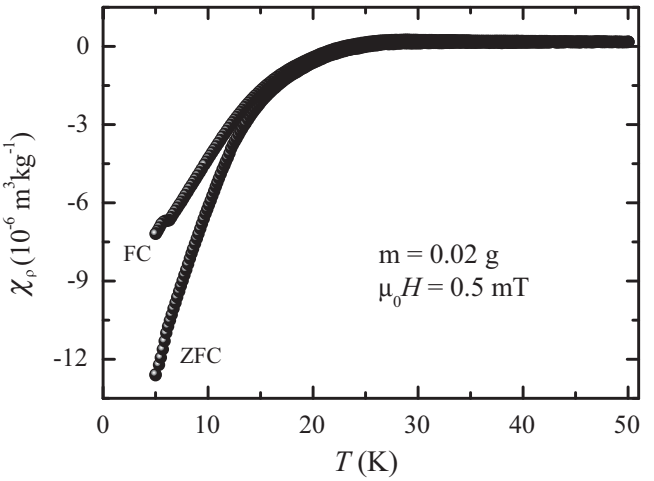

FIG. 4. Temperature dependence of the magnetic (mass) susceptibility for $Sm_4Fe_2As_2Te_{0.92(1)}O_4$ measured at 0.5 mT. FC is field cooled; ZFC is zero-field cooled.

*I*4/*mmm*). Like in 3442, the structure of 42214 consists of stacked fluorite-type L_2O_2 and anti-fluorite-type M_2Pn_2 layers. However, the sequence and numbers of the two types of layers are dissimilar for the two structures; furthermore, the atom in the center of the unit cell has a positive charge $L^{\delta+}$ for 3442 and negative charge $Te^{\delta-}$ for 42214. The two structures are isoconfigurational and have interchanged corresponding structure motifs: $(L_2O_2)_2(M_2Pn_2)Te$ vs $(L_2O_2)(M_2Pn_2)_2L$

TABLE III. Details of the structure refinement for the $L_4Fe_2As_2Te_{1-x}O_{4-y}F_y$ (L = Sm, Gd) crystals.

Empirical formula	$Sm_4Fe_2As_2Te_{0.72(1)}O_{4-y}F_y$	$Gd_4Fe_2As_2Te_{0.92(1)}O_{4-y}F_y$
T_c, K	40	45
Unit cell dimensions, Å, deg.	$a = 3.9597(5)$, $c = 29.268(5)$	$a = 3.9363(6)$, $c = 29.350(5)$
Volume, $Å^3$	458.89(11)	454.77(12)
L_1-L_2, Å	3.6413(6)	3.6124(10)
O-O = Fe-Fe, Å	2.7999(4)	2.7834(4)
L_2-As_1/L_1-Te, Å	3.2424(8)/3.4406(5)	3.2271(13)/3.4454(7)
L_2-O/L_1-O, Å	2.319(3)/2.275(3)	2.298(5)/2.263(5)
As_1-As_2, Å	3.8956(12)	3.9075(21)
Fe-As, Å	2.3987(7)	2.3987(12)
As_1-Fe-As_2, β (°)	108.59(2)	109.07(4)
As_2-Fe-As_3, α (°)	111.25(5)	110.27(8)
S_1, Å	2.330(4)	2.301(4)
$1/2S_2/h_p$, Å	1.355(3)	/1.370(3)
Fig. 1(a)		
S_3, Å	1.633(4)	1.635(4)
S_4, Å	1.999(4)	2.031(4)
Calculated density, g/cm^3	7.373	7.854
Absorption coefficient, mm^{-1}	37.614	41.938
F(000)	871	910
Crystal size, mm^3	0.024 × 0.118 × 0.179	0.033 × 0.054 × 0.065
Theta range for data collection, deg.	2.78 to 32.49	4.17 to 36.21
Index ranges	$-5 = <h<= 5$, $-5 = <k<= 5$, $-41 = <l<= 44$	$-4 = <h<= 6$, $-6 = <k<= 6$, $-42 = <l<= 48$
Reflections collected/unique	2293/301 $R_{int.} = 0.0559$	2294/390 $R_{int.} = 0.0365$
Completeness to 2theta	97.7%	97.5%
Data/restraints/parameters	301/0/20	390/0/19
Goodness-of-fit on F^2	1.253	1.215
Final R indices [I>2sigma(I)]	$R_1 = 0.0251$, w$R_2 = 0.0557$	$R_1 = 0.0422$, w$R_2 = 0.0982$
R indices (all data)	$R_1 = 0.0252$, w$R_2 = 0.0558$	$R_1 = 0.0433$, w$R_2 = 0.0987$

TABLE IV. Atomic coordinates and equivalent isotropic and anisotropic displacement parameters [Å^2 × 10^3] for the $L_4Fe_2As_2Te_{1-x}O_{4-y}F_y$.

Atom	Site	x	y	z L = Sm/Gd	U_{iso}	$U_{11} = U_{22}$	U_{33}
L_1	4*e*	½	½	0.0683(1)/0.0692(1)	10(1)/8(1)	8(1)/6(1)	13(1)/11(1)
L_2	4*e*	0	0	0.1479(1)/0.1476(1)	10(1)/8(1)	8(1)/8(1)	12(1)/10(1)
As	4*e*	½	½	0.2037(1)/0.2033(1)	11(1)/11(1)	11(1)/13(1)	11(1)/8(1)
Te	2*a*	0	0	0	16(1)/15(1)	11(1)/17(1)	11(1)/11(1)
Fe	4*d*	½	0	¼	11(1)/10(1)	14(1)/9(1)	14(1)/12(1)
O	8*g*	½	0	0.1066(2)/0.1072(2)	9(1)/6(2)	7(2)/3(4)	16(1)/12(4)

(Fig. 1(a)–1(e)), where L = Pr, Sm, Gd, and M = Fe, and Pn = As for the former and L = La, Ce, Nd, and M = Cu, Ni, and Pn = P for the latter. Regarding the definition from Lima-de-Faria *et al*. [25], the 42214 structure could be considered as an *anti*-$La_3Cu_4P_4O_2$-crystal structure.

The 3442 phase is considered as an ordered mixture of LMPnO and LM_2Pn_2 [11] (Fig. 2(c)–2(d)). The 42214 could be described as stacking of the 1111 structure with L_2O_2Te [26] (Fig. 1(a)–1(c)).

Across the lanthanide series, with increasing atomic number in the periodic table and decreasing covalent radius lattice constants, the thickness of the Pr_2O_2 layer, S_1, decreases while the thickness of the Fe_2As_2 layer, S_2 ($2 \times h_P$), increases (Fig. 3). The corresponding S_2 and S_3 layers are very close for both 1111 and 42214 structures [19] (Table I; Fig. 1(a)–1(c)), while the L_2O_2 (S_1) layer is thicker in 1111 by 0.1 Å. The h_P parameter increases monotonically from 1.332 to 1.366 Å and is getting, as was expected, close to the "optimal" value for $Sm_4Fe_2As_2Te_{1-x}O$ and $Gd_4Fe_2As_2Te_{1-x}O$ (1.352(3) and 1.366(3) Å, respectively).

The fluorine-doped crystals of $Sm_4Fe_2As_2Te_{1-x}O_{4-y}F_y$ and $Gd_4Fe_2As_2Te_{1-x}O_{4-y}F_y$ were also studied by single-crystal x-ray diffraction. The results are shown in Tables III and IV. In both cases, the lattice parameter c is smaller than for samples without fluorine. For $Sm_4Fe_2As_2Te_{1-x}O_{4-y}F_y$, c is much smaller, which could be caused by a high concentration of tellurium deficiency (about 28 at%). The lattice constants a and b for $Gd_4Fe_2As_2Te_{1-x}O_{4-y}F_y$ remain almost the same as for the sample without fluorine. For $Sm_4Fe_2As_2Te_{1-x}O_{4-y}F_y$, a and b are slightly smaller in comparison to $Sm_4Fe_2As_2Te_{1-x}O_4$. It is rather difficult to find any correlation or exact influence of fluorine doping with the lattice geometry because of different concentrations of vacancies in the Te site for each sample, as well as because of difficulties with estimation of the real fluorine content.

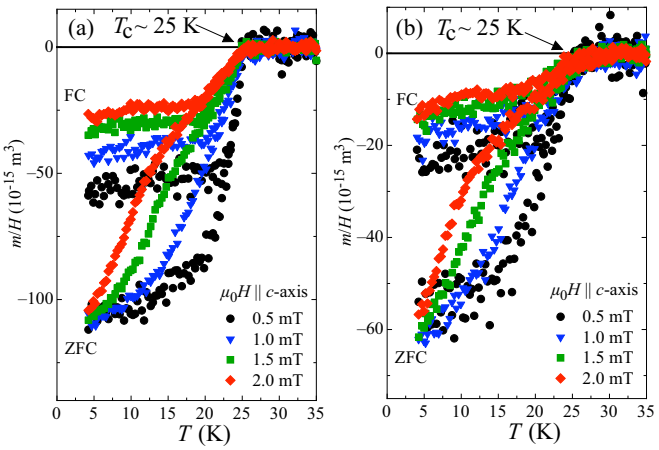

FIG. 5. (Color online) Temperature dependence of the magnetic susceptibility for: (a) $Pr_4Fe_2As_2Te_{0.88(1)}O_4$ and (b) $Gd_4Fe_2As_2Te_{0.90(1)}O_4$ single crystals.

B. Magnetic properties

1. *Samples with Te deficiency*

The temperature dependence of the magnetic susceptibility for the $Sm_4Fe_2As_2Te_{1-x}O_4$ powdered sample (m = 0.02 g) and

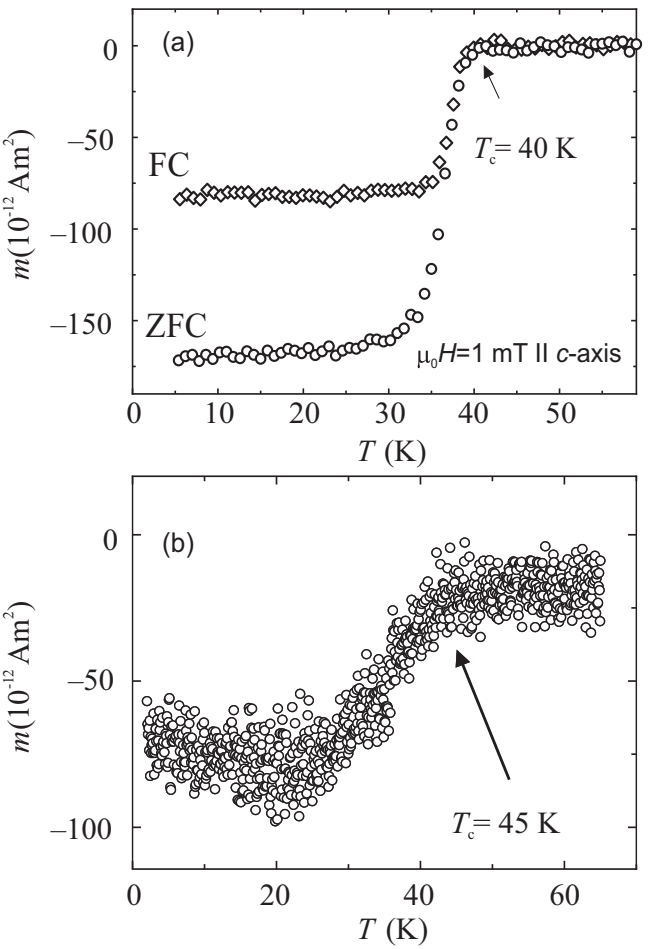

FIG. 6. Temperature dependence of the magnetization for: (a) $Sm_4Fe_2As_2Te_{0.72(1)}O_{4-y}F_y$ and (b) $Gd_4Fe_2As_2Te_{0.92(1)}O_{4-y}F_y$ single crystals.

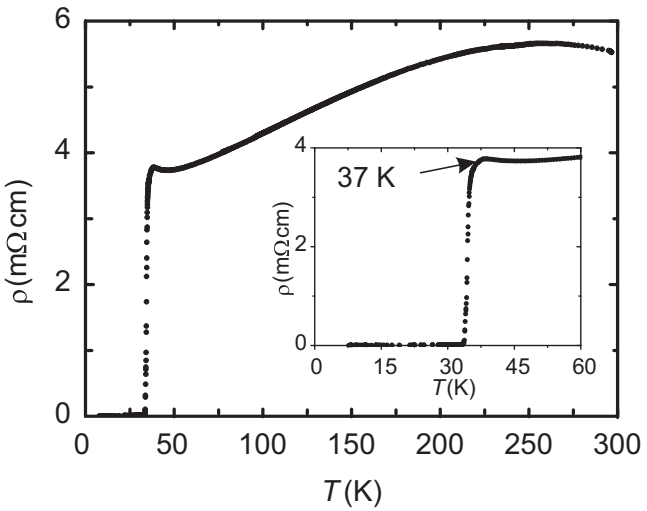

FIG. 7. Temperature dependence of the electrical resistivity for $Sm_4Fe_2As_2Te_{1-x}O_{4-y}F_y$ single crystal. Inset shows $\rho(T)$ around the superconducting transition.

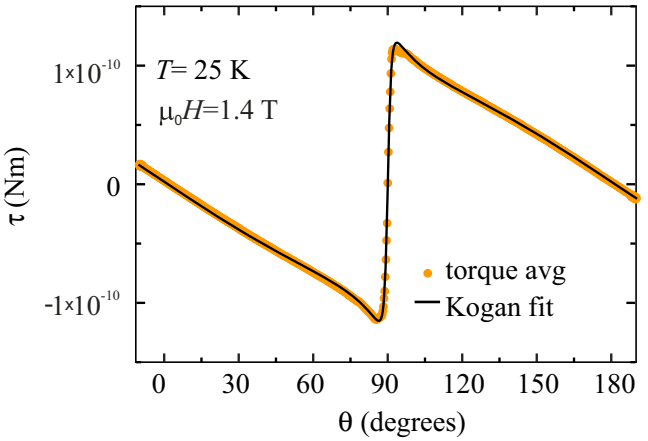

FIG. 8. (Color online) Torque as a function of the angle θ between the applied magnetic field H and the crystallographic c axis of a single crystal of $Sm_4Fe_2As_2Te_{0.72(1)}O_{4-y}F_y$ at $T = 25$ K and $\mu_0 H = 1.4$ T. The solid line denotes a fit according to the Kogan model from which the anisotropy parameter $\gamma = 31$ was extracted.

for two small individual single crystals of $L_4Fe_2As_2Te_{1-x}O_4$ (L = Pr, Gd) is shown in Figures 4 and 5, respectively. The $m/H(T)$ measurements for single crystals have been performed in various magnetic fields parallel to the c axis, for the ZFC and FC states. The observed signal reveals bulk superconductivity [12]. Magnetic measurements performed on the $Sm_4Fe_2As_2Te_{1-x}O_4$ powdered sample at an applied field of 0.5 mT showed the onset of superconducting transition at ~25 K, with a relatively small superconducting shielding fraction (9.4%; see the ZFC curve in Fig. 4, where the density of the compound was calculated to be 7.48 g/cm^3). The powdered sample was not single phase.

The onset of the superconducting transition for the $Sm_4Fe_2As_2Te_{1-x}O_4$ sample as well as for both single crystals of $L_4Fe_2As_2Te_{1-x}O_4$ (L = Pr, Gd) is estimated to be nearly the same, $T_c \sim 25$ K (Figs. 4–5). The omnipresent Te deficiency could be assumed as a doping causing superconductivity. The application of small magnetic fields above 1 mT already leads to a drastic broadening of the transition width, indicative of a very small lower critical field, H_{c1}.

2. *Samples with Te deficiency and doped with fluorine*

In Figure 6, the result of fluorine doping can be seen. Figure 6(a) shows *m(T)* for the ZFC and FC states of a single crystal of $Sm_4Fe_2As_2Te_{0.72(1)}O_{4-y}F_y$. After substituting nominally 30% of oxygen by fluorine, T_c increased from 25 K to 40 K. Figure 6(b) shows $m(T)$ for a $Gd_4Fe_2As_2Te_{0.92(1)}O_{4-y}F_y$ single crystal. Here, substitution of nominally 20% of oxygen by fluorine increased T_c up to 45 K. It is not clear if maximum T_c has been obtained. Doping dependence on T_c should be investigated in a broader range of compositions.

C. Transport measurement

The onset superconducting critical temperature is 36 K for $Sm_4Fe_2As_2Te_{1-x}O_{4-y}F_y$ (Fig. 7). The ρ-T curve suggests that the sample is not optimally doped and that some inhomogeneity is present in the structure. This might explain the small upturn in ρ just above the superconducting transition.

D. Magnetic torque studies

Figure 8 shows the torque as a function of the angle θ between the applied magnetic field H and the crystallographic c axis. When the field direction is swept clockwise (CW) and counterclockwise (CCW), a hysteresis between the CW and CCW torque curves appears. This is due to the pinning of the vortices on crystal defects [27]. The data shown here are the average of the CW and CCW curves.

The angular torque data are analyzed with the Kogan model [28], which allows the anisotropy γ of the material to be extracted. The anisotropy parameter γ is defined as λ_c/λ_{ab}, where λ_i is the magnetic field penetration depth for a field along the crystallographic i axis. The fit is done assuming a Werthamer-Helfand-Hohenberg [29] dependence of the upper critical field, with a slope at T_c given in Ref. [12].

The fit results in a rather high anisotropy of 31, measured at 25 K. This anisotropy is one of the highest among the iron-based superconductor family, consistent with the large distance between the superconducting Fe_2As_2 layers in this material.

IV. CONCLUSION

Single crystals of layered superconductors $L_4Fe_2As_2Te_{1-x}O_4$ (L = Pr, Sm, Gd; $x \sim 0.1$) were grown using the high-pressure cubic anvil technique. The structure reveals the stacking of anti-fluorite-type M_2Pn_2 and fluorite-type L_2O_2 layers, alternating with the chain of tellurium atoms, and it could be considered as an anti-$La_3Cu_4P_4O_2$-crystal structure. The critical temperature T_c is about 25 K and does not show any dependence on the kind of lanthanide atom.

Doping with fluorine increases T_c of $Sm_4Fe_2As_2Te_{1-x}O_{4-y}F_y$ up to 40 K and that of $Gd_4Fe_2As_2Te_{1-x}O_{4-y}F_y$ up to 45 K. For determination of maximum T_c of 42214, more detailed studies of T_c dependence on doping are necessary.

ACKNOWLEDGMENTS

This work was supported by the Swiss National Science Foundation (Project No. 140760) and by the European Community FP7 Super-Iron Project.

[1] Y. Kamihara, T. Watanabe, M. Hirano, and H. Hosono, J. Am. Chem. Soc. **130**, 3296 (2008).

[2] B. I. Zimmer, W. Jeitschko, Jr., H. Albering, R. Glaum, and M. Reehuis, J. Alloys Compd. **229**, 238 (1995).

[3] P. Quebe, L. J. Terbüchte, and W. Jeitschko, J. Alloys Compd. **302**, 70 (2000).

[4] G. Haegg and A. L. Kindstroem, Z. Physik. Chem. B Chem. Elementarproz., Aufbau Mat. **22**, 453 (1933).

[5] F. C. Hsu, J. Y. Luo, K. W. Yeh, T. K. Chen, T. W. Huang, P. M. Wu, Y. C. Lee, Y. L. Huang, Y. Y. Chu, D. C. Yan, and M. K. Wu, Proc. Natl. Acad. Sci. **105**, 14262 (2008).

[6] M. Pfisterer and G. Nagorsen, Z. Naturforsch. B **35**, 703 (1980).

[7] M. Rotter, M. Tegel, and D. Johrendt, Phys. Rev. Lett. **101**, 107006 (2008).

[8] R. Juza and K. Langer, Z. Anorgan. Allgem. Chem. **361**, 58 (1968).

[9] J. H. Tapp, Z. Tang, B. Lv, K. Sasmal, B. Lorenz, P. C. W. Chu, and A. M. Guloy, Phys. Rev. B **78**, 060505 (2008).

[10] R. J. Cava, H. W. Zandbergen, J. J. Krajewski, T. Siegrist, H. Y. Hwang, and B. Batlogg, J. Solid State Chem. **129**, 250 (1997).

[11] T. Klimczuk, T. M. McQueen, A. J. Williams, Q. Huang, F. Ronning, E. D. Bauer, J. D. Thompson, M. A. Green, and R. J. Cava, Phys. Rev. B **79**, 012505 (2009).

[12] S. Katrych, K. Rogacki, A. Pisoni, S. Bosma, S. Weyeneth, R. Gaal, N. D. Zhigadlo, J. Karpinski, and L. Forró, Phys. Rev. B **87**, 180508 (2013).

[13] K. Kuroki, H. Usui, S. Onari, R. Arita, and H. Aoki, Phys. Rev. B **79**, 224511 (2009).

[14] Y. Mizuguchi, Y. Hara, K. Deguchi, S. Tsuda, T. Yamaguchi, K. Takeda, H. Kotegawa, H. Tou, and Y. Takano, Supercond. Sci. Technol. **23**, 054013 (2010).

[15] T. Hanna, Y. Muraba, S. Matsuishi, N. Igawa, K. Kodama, S.-i. Shamoto, and H. Hosono, Phys. Rev. B **84**, 024521 (2011).

[16] K. Miyazawa, K. Kihou, P. M. Shirage, C.-H. Lee, H. Kito, H. Eisaki, and A. Iyo, J. Phys. Soc. Jpn. **78**, 034712 (2009).

[17] C. Wang, L. Li, S. Chi, Z. Zhu, Z. Ren, Y. Li, Y. Wang, X. Lin, Y. Luo, S. Jiang, X. Xu, G. Cao, and Z. Xu, Europhys. Lett. **83**, 67006 (2008).

[18] N. D. Zhigadlo, S. Katrych, S. Weyeneth, R. Puzniak, P. J. W. Moll, Z. Bukowski, J. Karpinski, H. Keller, and B. Batlogg, Phys. Rev. B **82**, 064517 (2010).

[19] J. Karpinski, N. D. Zhigadlo, S. Katrych, Z. Bukowski, P. Moll, S. Weyeneth, H. Keller, R. Puzniak, M. Tortello, D. Daghero, R. Gonnelli, I. Maggio-Aprile, Y. Fasano, Ø. Fischer, K. Rogacki, and B. Batlogg, Phys. C: Supercond. **469**, 370 (2009).

[20] Computer code APEX2, version 2009.9 (Bruker AXS Inc., Madison, Wisconsin, USA, 2009).

[21] Computer code SAINT, version 7.68A (Bruker AXS Inc., Madison, Wisconsin, USA, 2009).

[22] G. Sheldrick, Computer code SHELXS-97: Program for the Solution of Crystal Structures (University of Göttingen, Göttingen, Germany, 1997).

[23] G. Sheldrick, Computer code SHELXS-97: Program for the Refinement of Crystal Structures (University of Göttingen, Göttingen, Germany, 1997).

[24] S. Kohout, J. Roos, and H. Keller, Rev. Sci. Instrum. **78**, 013903 (2007).

[25] J. Lima-de-Faria, E. Hellner, F. Liebau, E. Makovicky, and E. Parthé, Acta Crystallogr. A **46**, 1 (1990).

[26] F. A. Weber and T. Schleid, Z. Anorgan. Allgem. Chem. **625**, 1833 (1999).

[27] M. Willemin, C. Rossel, J. Hofer, H. Keller, A. Erb, and E. Walker, Phys. Rev. B **58**, R5940 (1998).

[28] V. G. Kogan, Phys. Rev. B **38**, 7049 (1988).

[29] N. R. Werthamer, E. Helfand, and P. C. Hohenberg, Phys. Rev. **147**, 295 (1966).

[30] F. Nitsche, A. Jesche, E. Hieckmann, T. Doert, and M. Ruck, Phys. Rev. B **82**, 134514 (2010).

[31] J. Yang, X.-L. Shen, W. Lu, W. Yi, Z. C. Li, Z.-A. Ren, G.-C. Che, X.-L. Dong, L.-L. Sun, F. Zhou, and Z.-X. Zhao, New J. Phys. **11**, 025005 (2009).

[32] T. C. Ozawa and S. M. Kauzlarich, Sci. Tech. Adv. Mat. **9**, 033003 (2008).

[33] D. C. Johnston, Adv. Phys. **59**, 803 (2010).